Performance study of grid-connected Doubly-Fed Induction Generator controlled by an optimal controller under unbalanced condition

Shubha Baravani[1], Jaishri B. Veergoudar[2], Salma Shapurkar[3], Shreya Moholkar[4], Chetna Bhagoji[5]

[1]Associate Professor, Department of Electronics & Communication, Maratha Mandal Engineering College, Belagavi, Karnataka
[2]Assistant Professor, Department of Mathematics, KLE Technological University's Dr M. S. Sheshgiri College of Engineering and Technology, Belagavi
[3]Associate Professor, Department of Electronics & Communication, Jain College of Engineering Belagavi, Karnataka
[4]Assistant Professor, Department of Electrical Engineering, SVERI's College of Engineering, Pandharpur, Maharashtra
[5]Assistant Professor, Department of Applied Science, Maratha Mandal Engineering College, Belagavi, Karnataka

ABSTRACT

Effective addressing of the controller of a converter used in the doubly-fed induction generator (DFIG) under unbalanced grid voltage conditions is imperative. To reduce the effects of negative sequence voltages such as oscillatory components in the torque, negative sequence components in the stator and rotor current are required to add in the main control algorithm. In this study, an optimal control algorithm has been proposed for the achievement of various functional characteristics such as stator and rotor current, torque, active and reactive power of the DIFG. In addition, different scenarios for the designing of an optimal controller, an additional function is implemented to reduce the negative sequence has been proposed. The simulation was carried out using PLECS software. Detailed analysis was made to study the performance of the system. Simulation results illustrated the proposed optimal control algorithm improving the entire operational characteristic simultaneously. Finally, comparison has been done to study the performance of the proposed method with three other controllers. The comparison result showed the proposed optimal controller limiting the variations in the amplitude of negative sequence components of rotor current and negative sequence components of stator current to 1% and 1.4% respectively.

1. INTRODUCTION

There has been an exorbitant increase in the cost of fossil fuel during the last few decades. Various researchers and scientists found alternate sources of energy called renewable energy sources. Among the different types of wind generators, the variable speed wind generator called the doubly-fed induction generator (DFIG) had been found is most suitable. Economy in maintenance and high efficiency make DFIG better than other generators [1]. Nowadays, back-to-back converters (BBC) are widely used in wind energy conversion systems (WECS). They have several advantages such as the configuration of BBC enabling two side control (grid side and generator side), good controllability, and dealing with the bidirectional energy flow. Further, the BBC with an intermediate DC link provides guaranteed decoupling among generator and grid side [2]. A common control technique was developed by Tang et al. for the achievement of the bidirectional reactive and active power flow [3]. Creation of undesirable effect on the safety system was seen when the distributed generator was integrated with the main grid. This issue can be easily solved by the flexible control strategy of the BBC. In addition, the BBC wedged the micro grid when fault was identified, establishing smooth synchronization with the grid after correcting the fault [4], [5].

The grid side converter (GSC) can act as a rectifier for the regulation of DC voltage among the terminals of the coupling capacitor. In this study, machine side converter (MSC) was used for regulating the voltage while a GSC was used for control of the reactive and active power delivered to the grid [6]. For analyzing the faulty operations of the network and the transience in the normal mode has been studied by recording the d and q components of the feeder. The faulty and healthy mode of operation is identified within 2 ms [7]. During steady-state, the reference frame was seen having constant values of direct and quadrature current and voltages. The αβ0 transformation was used to detect the phase angle of the voltage for guaranteeing the decoupled control among active and reactive power [8].

Loss minimization and cost reduction are the major problems in power converters. This can be solved by modifying the topology of the converters or reduction in the semiconductor switches used [9]. A matrix converter has been proposed by Diaz et al. for WECS by including nine bidirectional switches with classical pulse width modulation (PWM) but not integrating a DC link capacitor [10]. The requirement of supplementary clamp circuit and the limitations of switching frequency has made the classical PWM as not suitable for the matrix converters (direct or indirect). The matrix converter functionality can be realized through use of eighteen switches. It requires additional six switches compared to BBC. On the other hand, it has other advantages such as life span extension due to removal of DC link capacitor and compactness developed a nine-switch indirect sparse matrix converter for WECS which supports a specific direction of power flow with the requirement of

constant frequency of operation. Hence, is not suitable for WECS [11]. Oscar have proposed a boost converter for PV system. Fuzzy logic-based boost converter was utilized a tracking method for obtaining maximum power for the PV system. The voltage, current, and power has been measured and compared with other methods [12].

Recently, the nine switch BBC has provided an alternative to the 12-switch BBCs. It increases the system efficiency, with reduction in cost, reduction in installation area, and less switching losses [13]. An experimental study conducted by Genu validated the nine switch converter for the dual machine drives works under both the fixed and variable frequencies [14]. Different modes of operation of a nine-switch converter with different modulation schemes have been proposed by Liu et al. [15]. This has been found to offer support for both the constant and variable frequencies. The lifetime of components gets reduced due to the torsional vibration induced by to the unbalanced grid voltage. Different researches focused on the subject of enhancement of the performance of the system [16]. The negative sequence components (NSC) have been considered for investigating the performance of the DFIG under voltage unbalanced condition (VUC) [17]. Moreover, the rotor converter gets damaged due to overcurrent. Hence, NSC of rotor current requires control to avoid such damages. In order to maintain the power quality, the oscillations created by the NSC in the reactive and active power should be minimized. Besides, limiting the active power oscillation (APO) leads to a decrease the oscillation of DC-link voltage. Various rotor current controllers have been proposed in prior studies for overcoming the unbalanced point of common coupling voltage [18]. Various researchers focused on NSC for both the GSC and MSC for management of the VUC of the grid. A study of the unwanted dynamics of the DFIG under VUC has also been made [19], [20]. The studies conducted by Dlzar et al. deal with regulation of both the negative and positive component of the MSC under VUC of an individual DFIG [21].

The controlling method of the DFIG generally depends on the application and the related problems. In a vector control method, the voltage dynamics (voltage-oriented reference frame of both the grid and stator) are directly control the GSC and MSC respectively [22]. In this paper, the optimized voltage-oriented vector control (OVVC) method has been proposed for nine switch back-to-back converters (OVVC-NBC) for controlling the voltage dynamics. Here, the state variables that include stator voltage and rotor current have been utilized. An optimization method has been used for the elimination of the torque pulsation, NSC in stator current (NSSC) and NSC in rotor current (NSRC). However, fluctuations in the DC-link voltage and rotor angular velocity of DFIG have not been considered as do not provide any significant effect on the percentage of oscillation on DFIG. The control objectives addressed are in terms of the dq components of the rotor current. To study the effectiveness of the proposed OVVC-NBC, five different state-of-art methods are compared and the result shows that the OVVC-NBC obtained the best result than other methods. In OVVC-NBC, the reference values of the controller have been selected via the multi-objective optimization framework. The contribution of the proposed OVVC-NBC is enumerated as follows:

- An optimized voltage-oriented vector control method has been proposed for nine switch back-to-back converters for controlling the positive and negative sequences.
- A multi-objective function for different control objectives has been defined. Non-linear load has been applied and a study of the performance of OVVC-NBC has been made.
- Performance comparison with other modern techniques has been conducted.

The remainder of the paper is structured as follows: Section 2 discusses the proposed system's model. Positive and negative sequence controlling method is described in section 3. Section 4 explains the simulation results. Section 5 provides the conclusion.

2. PROPOSED METHOD

Figure 1 is the schematic diagram of the proposed NSBC used in WECS. Through slip rings, the rotor windings of the DFIG are connected to the upper output terminals of the NSBC. The lower three terminals of the NSBC, on the other hand, are linked to the grid to allow power exchange between the grid and the rotor. Vector control based on speed sensor has been proposed in this study for the extraction of maximum power for the rated range of wind speed. A pinch control system was used to limit how fast the wind could blow, which kept the amount of wind power captured within WECS's rated capacity. The mathematical modeling of NSBC, mode of operation, and the modulation scheme are described in this section.

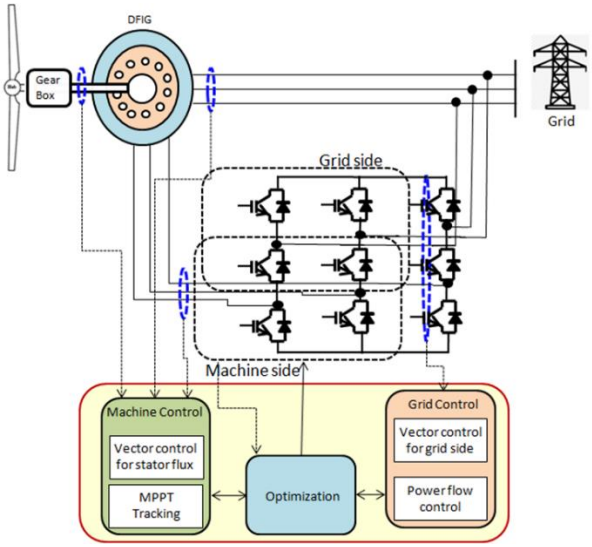

Figure 1. Proposed nine switch back-to-back converter for the WECS

2.1 Nine switch back-to-back converter

NSBC has three layers, namely, lower, middle, and upper layers. The lower layer consists of three power switches (S_1, S_2, S_3), the middle and upper layer has the power switches S_4, S_5, S_6, and S_7, S_8, S_9 respectively. The power switches on each layer have been linked one after the other to make three legs for the three phases. V_{dc} and 0 voltage is applied between (upper and lower layer) the parallel combination of power switches. The middle layer acts as a rectifier in conjunction with the upper and lower layer. It also shares the switches and supports for bi-directional operation. The component count is decreased from 12 to 9. As a result, a reduction in the percentage of component utilization is achieved as 33% and 50% for 12-switch BBC and 18-switch conventional converters respectively [23].

2.2 Model of DFIG

A control-oriented model is essential for the machine for a study of the dynamic behavior of DFIG. Because the rotor position is dependent on the coupled circuit model, the computing requirements are higher. This has motivated the author to utilize a two-axial model for the DFIG. The dq synchronous reference frame (dq-SRF) was used for exact control of the machine. The voltage and flux linkage equation of DFIG in dq-SRF can be expressed as:

$$v_{qr} = i_{qr}r_r + \frac{d\varphi_{qr}}{dt} + \varphi_{dr}\omega_r\,, \qquad v_{dr} = i_{dr}r_r + \frac{d\varphi_{dr}}{dt} - \varphi_{qr}\omega_r\,, \tag{1}$$

$$v_{qs} = i_{qs}r_s + \frac{d\varphi_{qs}}{dt} + \varphi_{ds}\omega_s\,, \qquad v_{ds} = i_{ds}r_s + \frac{d\varphi_{ds}}{dt} - \varphi_{qs}\omega_s\,, \tag{2}$$

$$\varphi_{qr} = i_{qr}S_r + S_m i_{qs}\,, \qquad \varphi_{dr} = i_{dr}S_r + S_m i_{ds}\,, \tag{3}$$

$$\varphi_{qs} = i_{qs}S_s + S_m i_{qr}\,, \qquad \varphi_{ds} = i_{ds}S_s + S_m i_{dr}\,, \tag{4}$$

where, $i_{ds}, i_{qs}, i_{dr}, and\ i_{qr}$ are the stator and rotor current of dq components. ω_s and ω_r denotes the synchronous angular speed and rotor speed respectively. $S_s, r_s, S_r, and\ r_r$ denote respectively the stator and rotor self-inductance and resistance. S_m is the mutual inductance of the stator and rotor windings. The zero sequence has not been considered because it does not present (zero sequences) unless there is an earth fault. Assuming the converter as lossless, the model of DC–link with the help of power equilibrium equation as:

$$P_{dc} + P_M + P_L = 0, \tag{5}$$

where, $P_{dc}, P_M\ and\ P_L$ are the active power of DC-link, active power at the line side and terminal side of the machine, respectively. Using [24], we can represent the active power components in the dq reference frame as,

$$P_{dc} = \frac{dW_{dc}}{dt} = \frac{d\left(\frac{1}{2}c\frac{dv_{dc}^2}{dt}\right)}{dt} = cv_{dc}\frac{dv_{dc}}{dt}, \tag{6}$$

where, c denotes the capacitance of DC-link. The DC-link dynamics can now be described as follows:

$$\frac{dv_{dc}}{dt} = \frac{-3}{2cv_{dc}}\left[\left(v_{dr}i_{dr} + v_{qr}i_{qr}\right) + \left(E_{qe}i_{qe} + E_{de}i_{de}\right)\right], \tag{7}$$

$$P_M = \frac{3}{2}Re\{v_r i_r^*\} = \frac{3}{2}\left(v_{dr}i_{dr} + v_{qr}i_{qr}\right) \tag{8}$$

$$P_L = \frac{3}{2}Re\{E_e i_e^*\} = \frac{3}{2}\left(E_{qe}i_{qe} + E_{de}i_{de}\right) \tag{9}$$

$v_{dr}\ and\ v_{qr}$ are the dq components of rotor voltage, v_{dc} is the DC-link voltage, $i_{de}\ and\ i_{qe}$ denote the dq components of the inverter output current, $E_{de} and\ E_{qe}$ are the dq components of inverter output voltage.

2.3 Extracting negative and positive sequence

Both the negative and positive sequences have parts that rotate at the same speed but in different directions. The stator current and voltage based on the reference frame of the positive sequence vector under voltage unbalance are given by

$$v = v^{+} + v^{-}(e^{-2j\omega_s t}) \quad (10)$$

$$i = i^{+} + i^{-}(e^{-2j\omega_s t}) \quad (11)$$

Therefore, the rotational speed has a difference of $-2\omega_s$. The voltage and current of the negative and positive components are 100 Hz signals, respectively when the synchronous frequency considered is $f_s = 50\,Hz$,. Hence, a notch filter has been used for the extraction of the 100 Hz signal from the dq signal consisting of both the negative and positive sequence signals. Similarly, the DC signal is extracted using a low-pass filter.

3. OPTIMAL CONTROL METHOD

This part gives a mathematical explanation of how the proposed system's performance will drop in situations where the voltage is always out of balance. This section provides the mathematical formulation of the performance deterioration of the proposed system under permanent voltage unbalanced (PVU) conditions. A controller is designed helped evaluation of the operation of negative sequence at MSC under PVU.

3.1 Extracting negative and positive sequence

The stator current and voltage based on the reference frame of the positive sequence vector under voltage unbalance are given by

$$v = v^{+} + v^{-}(e^{-2j\omega_s t}) \quad (11)$$

$$i = i^{+} + i^{-}(e^{-2j\omega_s t}) \quad (12)$$

Therefore, the rotational speed has a difference of $-2\omega_s$. The voltage and current of the negative and positive components are 100 Hz signals, respectively when the synchronous frequency considered is $f_s = 50\,Hz$,. As a result, a notch filter was employed to extract the 100 Hz signal from the dq signal, which included both the negative and positive sequence signals. Similarly, the DC signal is extracted using a low-pass filter.

3.2 Negative sequence voltage

The stator current and voltage can be expressed through selection of a positive sequence vector as reference frame under PVU as:

$$i^{+} = i_d^{+} + ji_q^{+},\ i^{-} = i_d^{-} + ji_q^{-},\ v^{+} = v_d^{+} + jv_q^{+}, v^{-} = v_d^{-} + jv_q^{-}, \quad (13)$$

where $i_d^{-}, i_q^{-}, v_d^{-}, and\ v_q^{-}$ denote respectively, the dq components of negative sequence current and voltage. $i_d^{+}, i_q^{+}, v_d^{+}, and\ v_q^{+}$ denote respectively the dq components of positive sequence current and voltage. By putting Equations 11, 12, and 13 into the power equation, one can estimate the active and reactive power as:

$$S_p = \frac{3}{2} v_s i_s^{*} = [P_{av} + P_1 \sin(2\omega_s t) + P_2 \cos(2\omega_s t) + j(Q_{av} + Q_1 \sin(2\omega_s t) + Q_2 \cos(2\omega_s t))] \quad (14)$$

where P_{av} is the average active power, $P_1 and\ P_2$ are amplitudes of the APO, $Q_1\ and\ Q_1$ are the peaks of the oscillating terms of the reactive power, Q_{av} is the average reactive power. P_{av} is expressed only in terms of positive sequence current and voltage. Suitable reference values have been calculated to compensate these oscillations. Eqn. 16 shows the appearance of the oscillatory terms in both the negative and positive sequences, the cosine and sine functions are used to represent the terms. On the other hand, Active and reactive power components were obtained by substituting stator and rotor current components. It can be written as:

$$\begin{bmatrix} P_{av} \\ Q_{av} \\ P_1 \\ P_2 \\ Q_1 \\ Q_2 \end{bmatrix} = \frac{3}{2S_s} \frac{1}{\omega_s} \left(\begin{bmatrix} -v_{qs}^{+} & v_{ds}^{+} & v_{qs}^{-} & -v_{ds}^{-} \\ v_{ds}^{+} & v_{qs}^{+} & -v_{ds}^{-} & -v_{qs}^{-} \\ -v_{qs}^{-} & v_{ds}^{-} & v_{qs}^{+} & -v_{ds}^{+} \\ v_{ds}^{-} & v_{qs}^{-} & v_{ds}^{+} & v_{qs}^{+} \\ v_{ds}^{-} & v_{qs}^{-} & -v_{ds}^{+} & -v_{qs}^{+} \\ v_{qs}^{-} & -v_{ds}^{-} & v_{qs}^{+} & -v_{ds}^{+} \end{bmatrix} \begin{bmatrix} v_{ds}^{+} \\ v_{qs}^{+} \\ v_{ds}^{-} \\ v_{qs}^{-} \end{bmatrix} - S_m \begin{bmatrix} v_{ds}^{+} & v_{qs}^{+} & v_{ds}^{-} & v_{qs}^{-} \\ v_{qs}^{+} & -v_{ds}^{+} & v_{qs}^{-} & -v_{ds}^{-} \\ v_{ds}^{-} & v_{qs}^{-} & v_{ds}^{+} & v_{qs}^{+} \\ v_{qs}^{-} & -v_{ds}^{-} & -v_{qs}^{+} & v_{ds}^{+} \\ v_{qs}^{-} & -v_{ds}^{-} & v_{qs}^{+} & -v_{ds}^{+} \\ -v_{ds}^{-} & -v_{qs}^{-} & v_{ds}^{+} & v_{qs}^{+} \end{bmatrix} \begin{bmatrix} i_{dr}^{+} \\ i_{qr}^{+} \\ i_{dr}^{-} \\ i_{qr}^{-} \end{bmatrix} \right) \quad (15)$$

In the same way, the electromagnetic torque (T_E) and the mechanical shaft power (P_M) is expressed as:

$$T_E = \frac{P}{2} \frac{P_M}{\omega_r} = T_{av} + T_1 sin(2\omega_s t) + T_2 cos(2\omega_s t), \quad (16)$$

$$P_M = \frac{3}{2} \frac{S_m P_e}{\omega_r} R_e\{-v_s i_r^{*}\} \quad (17)$$

where T_{av} is the average torque, $T_1 and\ T_2$ are oscillatory terms produced by the torque (TO). It can be expressed as:

$$\begin{bmatrix} T_{av} \\ T_1 \\ T_2 \end{bmatrix} = \frac{P}{2} \frac{3}{2} \frac{S_m}{S_s \omega_s} \begin{bmatrix} -v_{ds}^{+} - v_{qs}^{+} & v_{ds}^{-} & v_{qs}^{-} \\ v_{ds}^{-} & v_{qs}^{-} & -v_{ds}^{+} - v_{qs}^{+} \\ -v_{qs}^{-} & v_{ds}^{-} & v_{qs}^{+} & -v_{ds}^{+} \end{bmatrix} \begin{bmatrix} i_{dr}^{+} \\ i_{qr}^{+} \\ i_{dr}^{-} \\ i_{qr}^{-} \end{bmatrix} \quad (18)$$

From the above equations, it is observed that there is a straightforward connection among the dq stator current NSC and stator power oscillation; and straightforward relationship among the dq rotor current NSC and TO. Hence, power oscillation and torque reduction, reduction of NSC in stator and rotor current should be considered while designing controller. The NSC of stator current can be written as:

$$i_{qs}^{-} = \frac{1}{S_s}\left(-v_{ds}^{-} - S_m i_{qr}^{-}\right), i_{ds}^{-} = \frac{1}{S_s}\left(-v_{qs}^{-} - S_m i_{dr}^{-}\right), \quad (19)$$

T_E and active and reactive power in a synchronous stator voltage reference frame ($v_{qs}^{+} = 0$) can be estimated using the below equations

$$P_{av} = \frac{-3S_m}{S_s}\left(v_{ds}^{+} i_{dr}^{+} + v_{ds}^{-} i_{dr}^{-} + v_{qs}^{-} i_{qr}^{-}\right), \quad (20)$$

$$Q_{av} = \frac{3}{2S_s}\left[\left(v_{ds}^{+} v_{ds}^{+} - v_{ds}^{-} v_{ds}^{-} - v_{qs}^{-} v_{qs}^{-}\right) - S_s\left(-v_{ds}^{+} i_{dr}^{+} + v_{qs}^{-} i_{dr}^{-} - v_{ds}^{-} i_{qr}^{-}\right)\right] \quad (21)$$

$$T_{av} = \frac{-3PS_m}{4S_s\omega_s}\left(-v_{ds}^{+} i_{dr}^{+} + v_{ds}^{-} i_{dr}^{-} + v_{qs}^{-} i_{qr}^{-}\right), \quad (22)$$

where $i_{ds}^{-}, i_{qs}^{-}, i_{dr}^{-}, and\ i_{qr}^{-}$ are the dq components of negative sequence rotor and stator current. The controller is designed in such a way that it should eliminate all these components.

3.3 Design of an optimal controller

A controller for MSC has been designed for the control of the reactive and active power of DFIG. The rotor current dq components have been considered as the input variables. The d-axis was aligned with the stator voltage and the terminal voltage was seen as constant under steady-state conditions. Various scenarios for eliminating NSRC and NSSC are as follows:

- NSRC was eliminated by a proper setting of the reference values. $i_{dr}^{-*} = i_{qr}^{-*} = 0$.
- NSSC can be eliminated through setting of the reference values. $i_{ds}^{-} = 0 \rightarrow i_{dr}^{-*} = \frac{-1}{S_m} v_{qs}^{-}$, $i_{qs}^{-} = 0 \rightarrow i_{qr}^{-*} = \frac{1}{S_m} v_{qs}^{-}$
- To eliminate the oscillatory terms in torque through proper setting of the reference values as $T_1 = 0 \rightarrow i_{dr}^{-*} = \frac{1}{v_s^{+}}\left(i_{dr}^{+} v_{ds}^{-} + i_{qr}^{+} v_{qs}^{-}\right)$, $T_2 = 0 \rightarrow i_{qr}^{-*} = \frac{1}{v_s^{+}}\left(-v_{qs}^{-} i_{qr}^{+} + v_{ds}^{-} i_{qr}^{+}\right)$

3.4 Objective function

Pareto optimization method was used for the estimation of the optimal reference value. It is expressed as no solution is dominated by any other solution of a set of solutions. Use of this algorithm, helps sorting of the population into two phases. Initially, different Pareto fronts were recognized and sorted out on the basis of their Pareto front number. This was achieved through determination of the Pareto front for the complete population, while the previous one was removed when the next Pareto front is found. A secondary sorting method was used for sorting the Pareto front for obtaining the best solution [25]. Cooperation between all the objectives has been considered in the control strategies. The objective function for the optimization model is given by

$$Minimize: F(x) = \min\left(T_1, T_2, i_{ds}^{-}, i_{qs}^{-}, i_{dr}^{-}, i_{qr}^{-}\right) \quad (23)$$

The main aim of estimating the reference value was to minimize TO, simultaneously estimate the negative terms of both the stator current and rotor current.

4. RESULTS AND DISCUSSION

In this study, a 50 kV distribution system connected through a 40-km, 50 kV feeder which is linked with a 9 MW wind turbine system has been implemented using PLECS software. Different parameters of the turbine such as drivetrain, control system, turbine, and converter can be referred [26], [27] for more details. Extensive simulation tests have been executed in MATLAB software through setting of the reactive power P_{rea} and active reference power P_{act} as equal to zero and to the optimal mechanical power of the turbine respectively. Table 1 show various parameters used for the simulation.

4.1 Experimental Setup

The unbalance in the grid voltage is seen as less than 2% is considered. Up to 2% voltage unbalance the wind generator should not trip. The proposed optimal controller was seen maintaining the operational limit under 6% of the steady-state voltage. A study was made of the performance of the proposed controller under voltage condition (UVC). The simulation time was divided into three parts, namely, 1) positive sequence controller, 0 to 0.25 seconds with balanced grid voltage, 2) positive sequence controller, 0.25 to 0.6 seconds with unbalanced grid voltage, and 3) 0.6 to 0.9 seconds (unbalanced grid voltage with optimal controller).

Table 1. Various parameters used for simulation

DIFG	Controller

parameters	Value	parameters	Value
Nominal speed	1300 RPM		
Capacitor voltage	900 V	k_{Ω}	-900
Nominal power	9 MW	k_{ds}	-900
Stator voltage	3.8 kV	k_{qs}	-700
Capacitance	5500 µF	k_{xs}	-20
Mutual inductance Stator	25.15 mH	k_{ys}	-20
resistance	27.80 mΩ	Grid side controller	
Rotor inductance	27.15 mH	Voltage controller	
Stator inductance	26.20 mH		
Rotor resistance	26.25 mΩ	k_{vdc}	500
Grid frequency	50 Hz	k_{df}	7
Switching frequency	0.7 kHz	Current controller	
		k_{df}	7

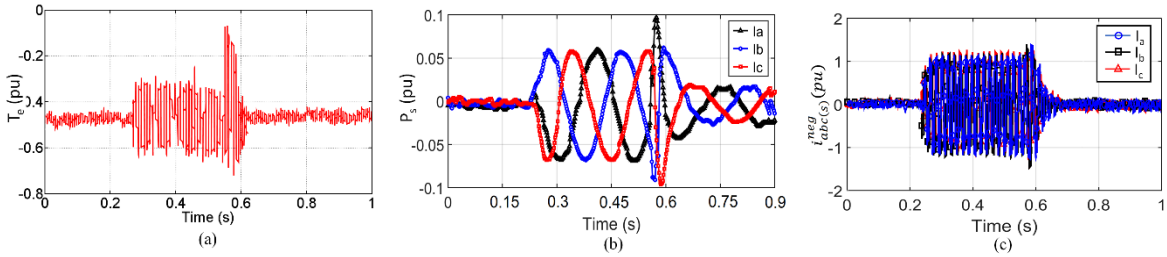

Figure 2. Elimination of rotor current negative sequence by the controller

4.2 Performance of OVVC-NBC

This subsection deals with the characteristics of the rotor current, the stator current, and the electromagnetic torque. The negative sequence grid voltage components created the negative sequence dq rotor current have been corrected by using the reference values. The performance of OVVC-NBC controller that eliminated the NSRC, NSSC, and the oscillatory component of torque are shown in Figures 2-4, respectively. Nonlinearity forced by another converter subsystem (filters, sub converters, etc.) creates oscillatory terms in the reactive and active power even underbalanced conditions. Moreover, the slip frequency changes the rotor current. The results illustrate the presence of the oscillatory terms such as Q_1, Q_2, and P_1, P_2 in the reactive and active powers due to negative sequence current and voltage under UVC. Eqn. 13 and 14 indicate the active and reactive power having different oscillatory terms. In addition, deviations of the average values of reactive and active powers are deviated from the negative voltage sequences are seen.

4.3 Performance at MSC

The response of WECS under the OVVC-NBC method is shown in Figure 5 as also the speed of the wind, speed of DFIG, total electromagnetic torque, mechanical power, and voltage and current of DFIG. The performance of the proposed OVVC-NBC is tested when the wind turbulence is applied at t=10 s. The DFIG makes a perfect tracking of its optimum speed even with heavy fluctuation in the wind. When wind speed exceeds its rated value the optimal controller limits the speed of the DFIG. The total electromagnetic torque and the mechanical power generated by the DFIG are shown in Figures 5(c)-(d). It is noticed that the variation in the total for the same speed of the incoming wind. When the wind speed reaches its rated value, the maximum power is extracted. Figure 5(e) depicts a phase voltage and its related current. As observed, the current waveform is sinusoidal and nearly in phase with the phase voltage.

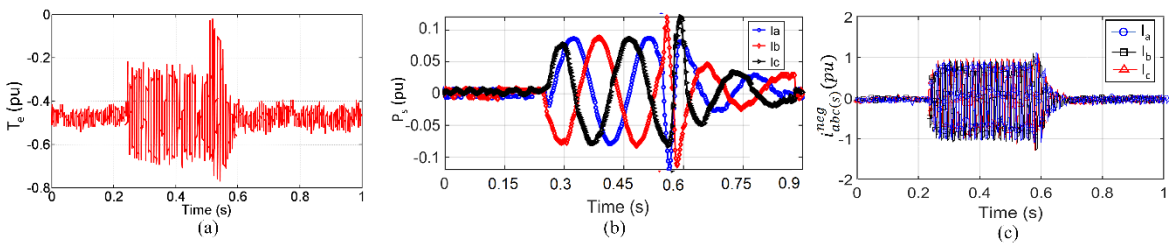

Figure 3. Elimination of stator current negative sequence by the controller

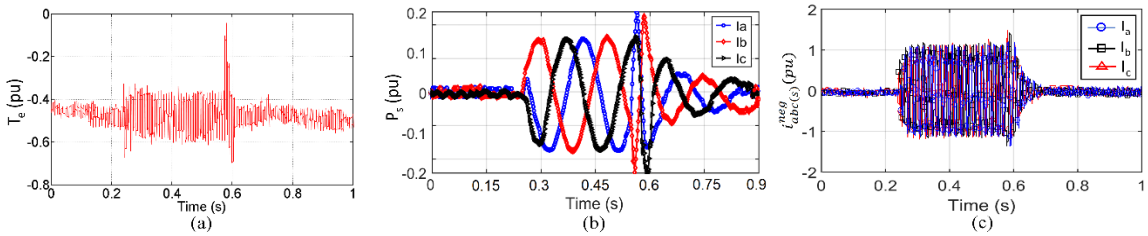

Figure 4. Elimination of oscillatory component of torque by the controller

4.4 Performance of nonlinear load

The nonlinear load was applied to WECS and the response is shown in Figure 6. In the experiment, a 3-φ rectifier was linked to the point of common coupling at t=1.5 s and removed at t=6.75 s. Figure 6 shows the inverter current, current injected to the load, and load current. The load coupling is seen as not affecting inverter current. On the other hand, a portion of generated current was absorbed by the nonlinear load as a result reduction in the magnitude of the injected current to the grid. The obtained results show the OVVC-NBC providing a better performance under nonlinear load conditions.

4.5 Performance comparison

The oscillations in the operational characteristics of the DFIG caused by the voltage unbalance should be minimized. Voltage unbalance was computed before introducing the negative voltage sequence for the evaluation of the percentage of reduction in oscillation. Maximum deviation from their average was deducted in the presence of negative voltage sequence after introducing optimal controller under steady-state condition [28], [29].

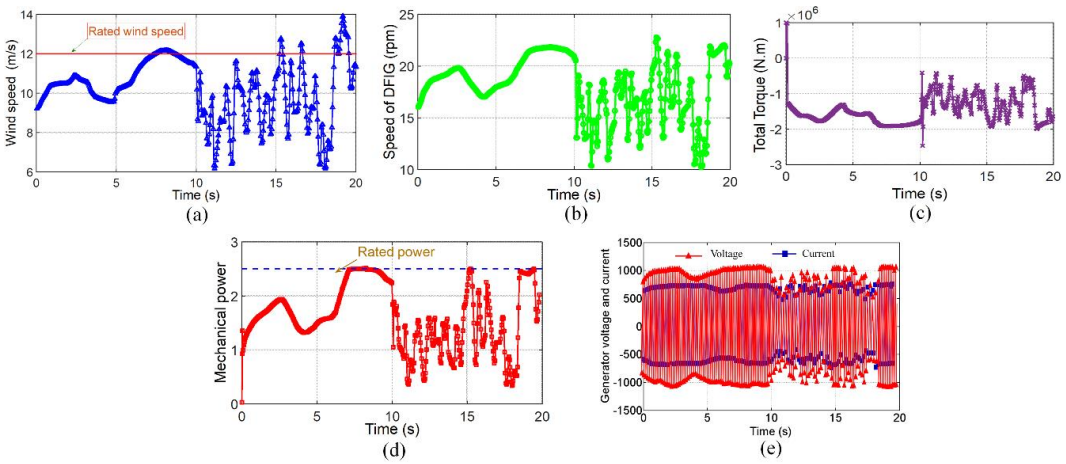

Figure 5. Simulation results of DFIG wind system controller by OVVC-NBC (MSC): (a) speed of wind (b) speed of DFIG (c) total electromagnetic torque (d) mechanical power (e) voltage and current of DFIG.

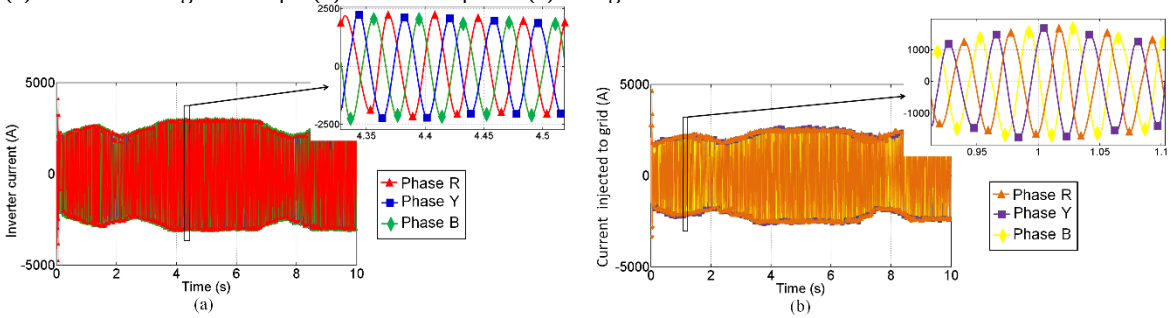

Figure 6. Simulation results of DFIG wind system controller by OVVC-NBC (GSC): (a) inverter current (b) injected current to the grid.

The presence of the grid UVC with a positive controller is seen between t=0.25 to 0.6 seconds (refer to Figures 2-4). Limits of 4% for stator/rotor current, active/reactive power, and 2% for torque oscillation were allowed for the fulfillment of the standard limit and preventing any damage. The performance of the proposed optimal controller including voltage unbalance of 6% is shown in Figure 7. The negative sequence in the rotor current

increased by 9.95%. The performance of OVVC-NBC has been compared with that of each of three other state-of-the-art controllers (PI, PID, and FOPID).

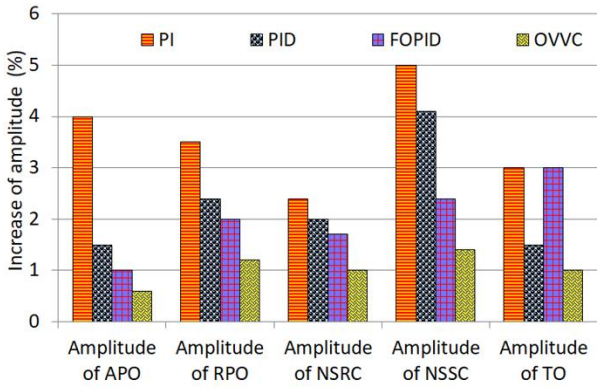

Figure 7. Comparison of negative sequence controllers and optimal controller for different operational characteristics.

The proposed optimal controller was seen adjusting the characteristics of current, power, and torque simultaneously. The amplitudes of NSRC and NSSC were limited to 1% and 1.4%, respectively. The peak oscillation of active and reactive power and torque was limited to 1%.

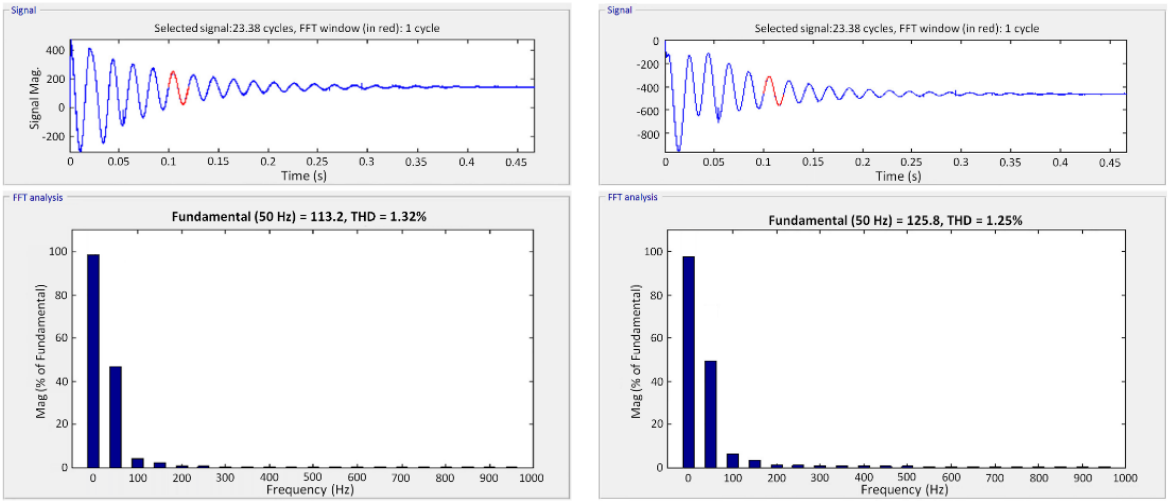

(a) (b)

Figure 8. THD analysis (a) MSC and (b) GSC

The harmonic spectrum of the rotor current for the proposed OVVC-NBC used in the wind energy conversion system is shown in Figure 8(a). The harmonic distortion obtained for MSC is seen as 1.32%. The harmonic spectrum of grid-side current for the proposed OVVC-NBC is shown in Figure 8(b). The harmonic distortion obtained is seen as 1.25%. The grid current is seen as close to sinusoidal due to the impact of harmonic reduction.

5. CONCLUSION

In this research, an optimal controller for the regulation of a DFIG-based wind turbine system is given. The working characteristics of DFIG improved under the permanent unbalance of grid voltage. The simulation period was split into three parts (t=0 to 0.25 s, t=0.25 to 0.6 s, and t=0.6 to 0.9). The proposed algorithm has been controlling the oscillatory components in the torque, negative sequence component in the stator current, and rotor current. This was achieved by the use of a multi-objective optimization method. A study of the performance of the proposed controller was made in the presence of negative sequence voltage. The experiment was conducted with a standard allowable limit of 4% of stator/rotor current, active/reactive power and 2% for torque oscillation. The simulation result showed the proposed optimal controller maintaining the allowable limit for all the operational characteristics and controlling all the parameters. Finally, a performance comparison was carried out between the proposed controller and three other controllers (PI, PID, and FOPID). The comparison result showed the proposed optimal controller limiting the variations in the amplitude of NSRC

and NSSC to 1% and 1.4%, and the amplitude variation of active and reactive power and torque is limited to 1%.

References

[1] R. Kumar, S. Das and A. Bhaumik, "Speed sensorless model predictive current control of doubly-fed induction machine drive using model reference adaptive system", *ISA Transactions*, vol. 86, pp. 215-226, 2019. DOI: 10.1016/j.isatra.2018.10.025.
[2] H. Yoo, T. Nguyen and H. Kim, "Multi-Frequency Control in a Stand-Alone Multi-Microgrid System Using a Back-To-Back Converter", *Energies*, vol. 10, no. 6, p. 822, 2017. DOI: 10.3390/en10060822.
[3] C. Tang, Y. Chen, Y. Chen and Y. Chang, "DC-Link Voltage Control Strategy for Three-Phase Back-to-Back Active Power Conditioners", *IEEE Transactions on Industrial Electronics*, vol. 62, no. 10, pp. 6306-6316, 2015. DOI: 10.1109/tie.2015.2420671.
[4] K. Tawfiq, A. Mansour, H. Ramadan, M. Becherif and E. El-kholy, "Wind Energy Conversion System Topologies and Converters: Comparative Review", *Energy Procedia*, vol. 162, pp. 38-47, 2019. DOI: 10.1016/j.egypro.2019.04.005.
[5] Y. Ding, M. Mao and L. Chang, "Conservative power theory and its applications in modern smart grid: Review and prospect", *Applied Energy*, vol. 303, p. 117617, 2021. DOI: 10.1016/j.apenergy.2021.117617.
[6] E. Chetouani, Y. Errami, A. Obbadi and S. Sahnoun, "Optimal tuning of PI controllers using adaptive particle swarm optimization for doubly-fed induction generator connected to the grid during a voltage dip", *Bulletin of Electrical Engineering and Informatics*, vol. 10, no. 5, pp. 2367-2376, 2021. DOI: 10.11591/eei.v10i5.2843.
[7] R. Dashti, M. Daisy and M. Aliabadi, "Healthy and faulty mode detection in power distribution networks based on park transformation", *Electric Power Systems Research*, vol. 191, p. 106867, 2021. DOI: 10.1016/j.epsr.2020.106867.
[8] Hajizadeh, "Stability Analysis and Optimal State Feedback Control of Back-to- Back Converter", *Journal of Technology Innovations in Renewable Energy*, 2013. DOI: 10.6000/1929-6002.2013.02.02.6.
[9] M. Felzke Schonardie, R. Francisco Coelho, L. Schmitz and D. Cruz Martins, "Active And Reactive Power Control in a Three-phase Grid-connected PV Power System Using Dq0 Transformation", *Eletrônica de Potência*, vol. 18, no. 4, pp. 1180-1187, 2013. DOI: 10.18618/rep.2013.4.11801187.
[10] M. Diaz et al., "Control of Wind Energy Conversion Systems Based on the Modular Multilevel Matrix Converter", *IEEE Transactions on Industrial Electronics*, vol. 64, no. 11, pp. 8799-8810, 2017. DOI: 10.1109/tie.2017.2733467.
[11] T. Elango and A. Senthil Kumar, "Voltage regulation of a stand-alone self-excited induction generator using STATCON with one cycle control technique for wind energy conversion system", *International Journal of Ambient Energy*, vol. 38, no. 5, pp. 497-508, 2016. DOI: 10.1080/01430750.2015.1132769.
[12] O. ZONGO, "Comparing the Performances of MPPT Techniques for DC-DC Boost Converter in a PV System", *Walailak Journal of Science and Technology (WJST)*, vol. 18, no. 2, 2021. DOI: 10.48048/wjst.2021.6500.
[13] S. Datta, J. Mishra and A. Roy, "Operation and control of a DFIG-based grid-connected WECS using NSC during grid fault and with unbalanced non-linear load", *International Journal of Ambient Energy*, vol. 39, no. 7, pp. 732-742, 2017. DOI: 10.1080/01430750.2017.1345008.
[14] L. Genu, L. Limongi, M. Cavalcanti, F. Bradaschia and G. Azevedo, "Single-phase transformerless power conditioner based on a two-leg of a nine-switch converter", *International Journal of Electrical Power & Energy Systems*, vol. 117, p. 105614, 2020. DOI: 10.1016/j.ijepes.2019.105614.
[15] X. Liu, P. Wang, P. Loh and F. Blaabjerg, "A Compact Three-Phase Single-Input/Dual-Output Matrix Converter", *IEEE Transactions on Industrial Electronics*, vol. 59, no. 1, pp. 6-16, 2012. DOI: 10.1109/tie.2011.2146216.
[16] A. Bakbak et al., "PMSG-Based Dual-Port Wind-Energy Conversion System With Reduced Converter Size", *IEEE Access*, vol. 9, pp. 118953-118967, 2021. DOI: 10.1109/access.2021.3107595.
[17] A. Leon, J. Mauricio and J. Solsona, "Fault Ride-Through Enhancement of DFIG-Based Wind Generation Considering Unbalanced and Distorted Conditions", *IEEE Transactions on Energy Conversion*, vol. 27, no. 3, pp. 775-783, 2012. DOI: 10.1109/tec.2012.2204756.
[18] A. Luna, F. Lima, D. Santos, P. Rodriguez, E. Watanabe and S. Arnaltes, "Simplified Modeling of a DFIG for Transient Studies in Wind Power Applications", *IEEE Transactions on Industrial Electronics*, vol. 58, no. 1, pp. 9-20, 2011. DOI: 10.1109/tie.2010.2044131.
[19] R. Arindya, "A Variable Speed Wind Generation System Based on Doubly Fed Induction Generator", *Bulletin of Electrical Engineering and Informatics*, vol. 2, no. 4, 2013. DOI: 10.12928/eei.v2i4.193.
[20] X. Chen and X. Wang, "Operation and Control of Stand-alone Brushless Doubly Fed Induction Generator Using Control Winding Side Converters", *Electric Power Components and Systems*, vol. 44, no. 9, pp. 1051-1062, 2016. DOI: 10.1080/15325008.2016.1148081.
[21] D. Al kez et al., "A critical evaluation of grid stability and codes, energy storage and smart loads in power systems with wind generation", *Energy*, vol. 205, p. 117671, 2020. DOI: 10.1016/j.energy.2020.117671.
[22] L. Rodrigues, J. Solis-Chaves, O. Vilcanqui and A. Filho, "Predictive Incremental Vector Control for DFIG With Weighted-Dynamic Objective Constraint-Handling Method-PSO Weighting Matrices Design", *IEEE Access*, vol. 8, pp. 114112-114122, 2020. DOI: 10.1109/access.2020.3003285.
[23] O. Kwon, J. Kwon and B. Kwon, "Highly Efficient Single-Phase Three-Level Three-Leg Converter Using SiC mosfets for AC–AC Applications", *IEEE Transactions on Industrial Electronics*, vol. 65, no. 9, pp. 7015-7024, 2018. DOI: 10.1109/tie.2018.2793231.
[24] S. Marmouh, M. Boutoubat, L. Mokrani and M. Machmoum, "A coordinated control and management strategy of a wind energy conversion system for a universal low-voltage ride-through capability", *International Transactions on Electrical Energy Systems*, vol. 29, no. 8, 2019. DOI: 10.1002/2050-7038.12035.
[25] K. Qu, T. Yu, X. Zhang and H. Li, "Homogenized adjacent points method: A novel Pareto optimizer for linearized multi-objective optimal energy flow of integrated electricity and gas system", *Applied Energy*, vol. 233-234, pp. 338-351, 2019. DOI: 10.1016/j.apenergy.2018.10.037.
[26] G. R, "Wind Farm-DFIG Detailed Model", 2022. [Online]: https://www.mathworks.com/help/sps/ug/wind-farm-dfig-detailed-model.html;jsessionid=566e4a2e5e975d52b22c0dc1a2e2. [Accessed: 28- Sep- 2022].
[27] J. Liu, Z. Yang, J. Yu, J. Huang and W. Li, "Coordinated control parameter setting of DFIG wind farms with virtual inertia control", *International Journal of Electrical Power & Energy Systems*, vol. 122, p. 106167, 2020. DOI: 10.1016/j.ijepes.2020.106167.
[28] Special Assessment. *Interconnection Requirements for Variable Generation*. Washington, D.C.: The World Bank, 2012.
[29] S. Reddy and P. Bijwe, "Real time economic dispatch considering renewable energy resources", *Renewable Energy*, vol. 83, pp. 1215-1226, 2015. DOI: 10.1016/j.renene.2015.06.011.